SUPPORTING INFORMATION

Eggshell-derived Nanoparticles Accelerate Wound Healing

Proma Nagchowdhury[a,b], Swapnali Londhe[a,b], Sanchita Tripathy[a,b], Yogesh Chandra[a,b], Chitta Ranjan Patra*[a,b]

[a]Department of Applied Biology, CSIR-Indian Institute of Chemical Technology, Uppal Road, Tarnaka, Hyderabad - 500007, Telangana State, India.

[b]Academy of Scientific and Innovative Research (AcSIR), Ghaziabad- 201002, India.

***To whom correspondence should be addressed**
Chitta RanjanPatra, Ph.D.
Chief Scientist
Department of Applied Biology,
CSIR-Indian Institute of Chemical Technology,
Uppal Road, Tarnaka, Hyderabad - 500007, Telangana State, India
Tel: +91-40-27193153
E-mail: crpatra.iict@csir.res.in

2. Experimental procedures

2.1. Synthesis and characterization of ES-NP

In order to perform all *in vitro* and *in vivo* experiments for the present manuscript, we have again synthesized ES-NP as per our earlier published report.[1] In this manuscript, the unfertilized and fertilized egg shell nanoparticles are abbreviated as U-ES-NP and F-ES-NP, respectively. Both U/F-ES-NP were synthesized according to our previously published report.[1] Both U/F-ES-NP are abbreviated in general as ES-NP. The eggshells after cleaning and washing were subjected to calcination at 700 °C to form ES-NP. The ES-NP (new batch) were characterized using several analytical techniques (including DLS, XRD, TEM, SEM, FE-SEM, FT-IR, TGA & DTG, etc.) as per our our published lietrature.[1] The detailed procedures for characterization techniques for the newly synthesized ES-NP are provided below.

2.1.1. X-Ray Diffraction (XRD)

The XRD technique was employed to study the crystallographic structure of the eggshell-derived nanoparticles. The white powder of calcined ES-NP obtained were evaluated by the X-Ray powder diffraction method with Bruker AXS D8 Advance Powder X-ray diffractometer (where CuKαλ=1.5406Å radiation).

2.2.2 Dynamic Light Scattering (DLS)

DLS technique was employed to analyze the hydrodynamic diameter (size) and zeta potential (charge) of ES-NP. The stock solutions of ES-NP (1mg/mL) were dissolved in Milli-Q water in a ratio of 1:9 (v/v) for the analysis of particle size and charge by DLS instrument Litesizer 500 Particle Analyzer (Anton Par).

2.2.3 Transmission Electron Microscopy (TEM) and Energy Dispersive X-Ray (EDAX)

The TEM analysis was performed to study the particle size, composition, and morphology of the nanoparticles. The white powder of ES-NP samples were dissolved in Milli-Q water (1mg/mL). A drop of this mixture was placed onto a copper grid with carbon coat. The grid was then allowed to dry before being examined using TEM and EDAX analysis by TEM: Tecnai G2 F30 S-Twin Microscope operated at 100kV.

2.2.4. Scanning Electron Microscopy (SEM) and Field Emission Scanning Electron Microscopy (FESEM)

To examine the microstructural surface morphology and composition of the ES-NP, scanning electron microscopy (SEM) analysis was. The ES-NP was analyzed by SEM Hitachi S-3000N, Japan. For FESEM analysis, specimens were mounted in horizontal and lateral positions to study the detailed surface topography and fractured cross-sections of ES-NP for evaluating homogeneity. Field Emission Scanning Electron Microscope (FESEM) study was performed on moisture-cured JEOL 7610F model (FE-SEM).

2.2.5. Fourier transformed infrared (FT-IR) spectroscopy

The FTIR technique was carried out for the ES-NP to evaluate the functional groups present in these samples. The dried powder of ES-NP samples were analyzed for the FTIR technique. The spectra were recorded by thermos Nicolet Nexus 670 spectrometer scanning at the range of 550-4000 cm^{-1} in diffuse reflectance mode in KBr pellets.

2.2.6. Thermogravimetric Analysis (TGA) and Derivative of Thermogravimetric Analysis (DTG)

The thermal stability of the ES-NP was studied as per previously published literature, using (TGA/Q500, from TA Instruments, USA) from 25 to 800 °C at 10 °C/min in nitrogen atmosphere.

2.3. *In vitro* assays

2.3.1 Cell viability assay using MTT reagent

The cell viability experiment of HaCaT and L929 cell lines in the presence of eggshell nanomaterials (ES-NP) using MTT reagent was performed as per our published literature [for detailed procedure, see Supporting Information (SI)][1]. Initially, 7×10^3 cells/well were seeded in 96 well plates with DMEM complete media and were kept for 24 h till confluence. Later, the cells were incubated with U/F-ES-NP (1-20 µg/mL) for a period of 24 h. Further, to understand whether the reactive oxygen species (ROS) generated by the cells helps to mimic keratinocyte proliferation, we incubated HaCaT cells with H_2O_2 for 2 h (10-50 µM), followed by replacement of fresh media for another 24 h. The media of each well was then replaced with 0.5% MTT containing fresh media (0.5 mg/mL in DMEM) and incubated for 4 h in the

dark at 37 °C. The media was then replaced with DMSO: Methanol (1:1; v/v) solution to solubilize the formed formazan crystals. The absorbance of the samples was measured at 570 nm with Synergy H1 multimode plate reader system.

2.3.2. Immunocytochemistry (Ki-67 & CD44)

The immunocytochemistry analysis (Ki-67 & CD44) was performed in HaCaT cell line using eggshell nanoparticles (ES-NP) as per our published literature (for detailed procedure, see SI) [2]. Briefly, the HaCaT cells (around 1×10^5) were seeded onto coverslips in a 6 well plate and grown till 50–60% confluence. The cells were then treated with U/F-ES-NP (5 µg/mL) for 24 h. Later, the cells were washed thrice with PBS and fixed with 4% paraformaldehyde for 10 mins. Again, the samples were washed with PBS, permeabilized with 0.2% Triton X followed by blocking the nonspecific sites with 3% bovine serum albumin in TBST (1X) buffer for 1 h at room temperature. The cells were incubated with anti-Ki-67, or anti-CD44 primary antibody for overnight at 4°C. Next day, the coverslips were washed with TBST and incubated with corresponding secondary antibody conjugated with Alexa Fluor 594 in the dark for 1 h at room temperature. The cells were washed with 1X TBST to remove the unbound antibody solutions and incubated for 10 min with DAPI (nuclear staining). Finally, the fluorescence images of the stained cells were captured using Nikon TiEclipse (TE 2000-E, Japan) Confocal Microscope at 60 × magnification.

Figure S1.

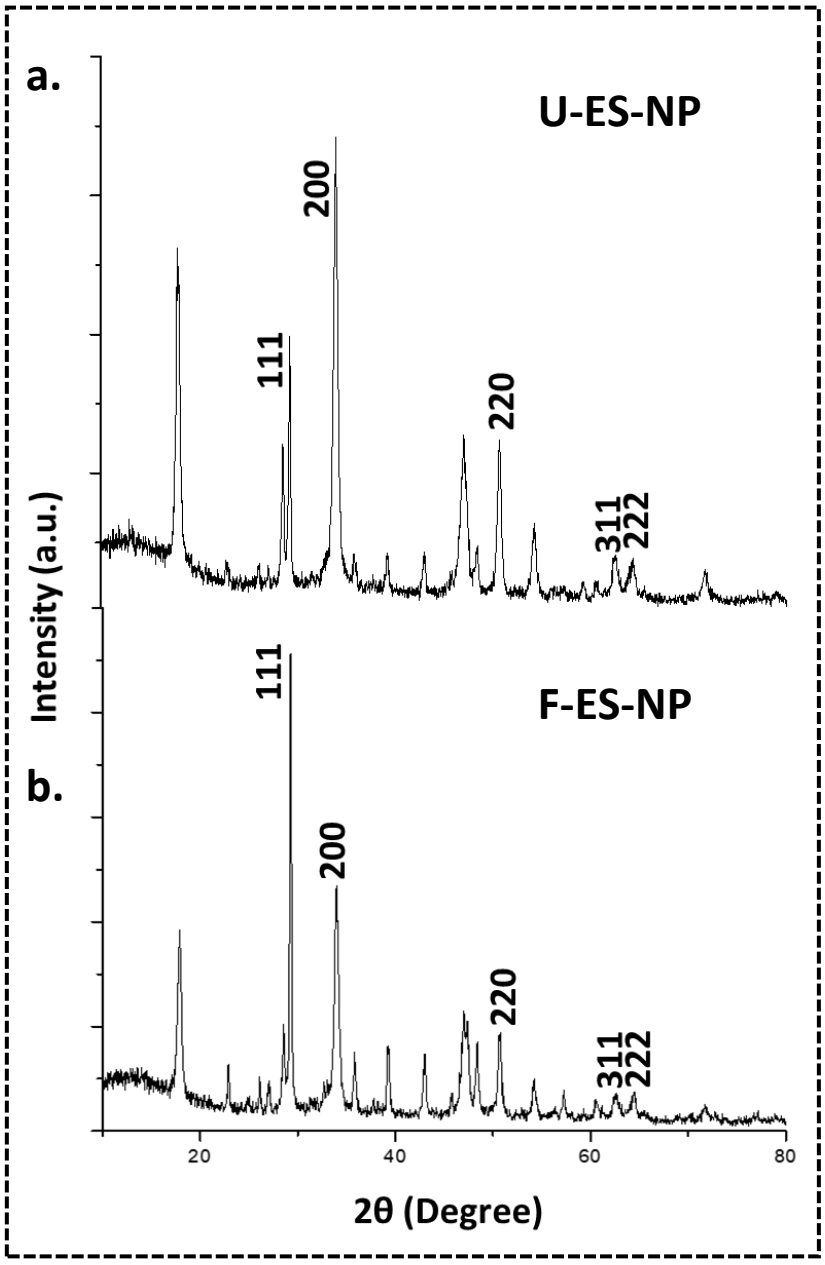

Figure S1. XRD spectra of: **(a)** U-ES-NP; **(b)** F-ES-NP. The results indicate the polycrystalline nature of all of these samples.

Figure S2

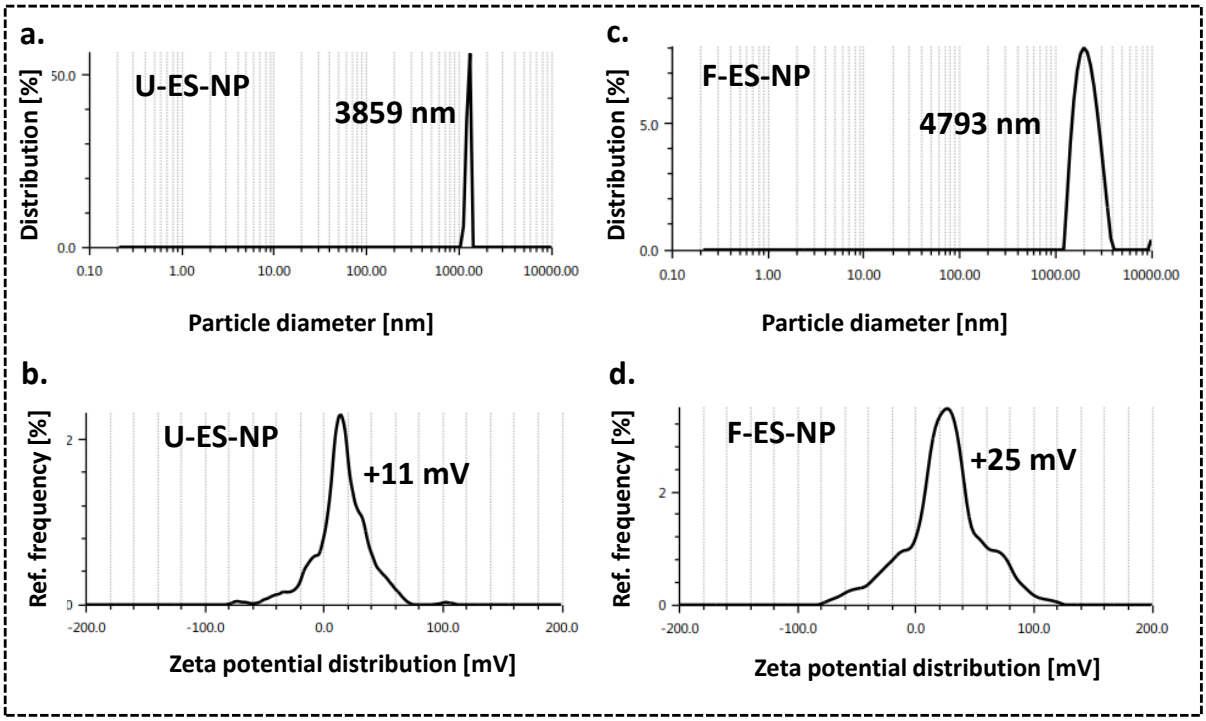

Figure S2. DLS analysis of: **(a,b)** U-ES-NP; and **(c,d)** F-ES-NP. Hydrodynamic diameter (size) of U-ES-NP is: **(a)** ~3859 nm; and zeta potential (charge) of U-ES-NP is: **(b)** +11 mV. Hydrodynamic diameter (size) of F-ES-NP is: **(c)** ~4793 nm; and zeta potential (charge) of F-ES-NP is: **(d)** +25 mV.

Figure S3.

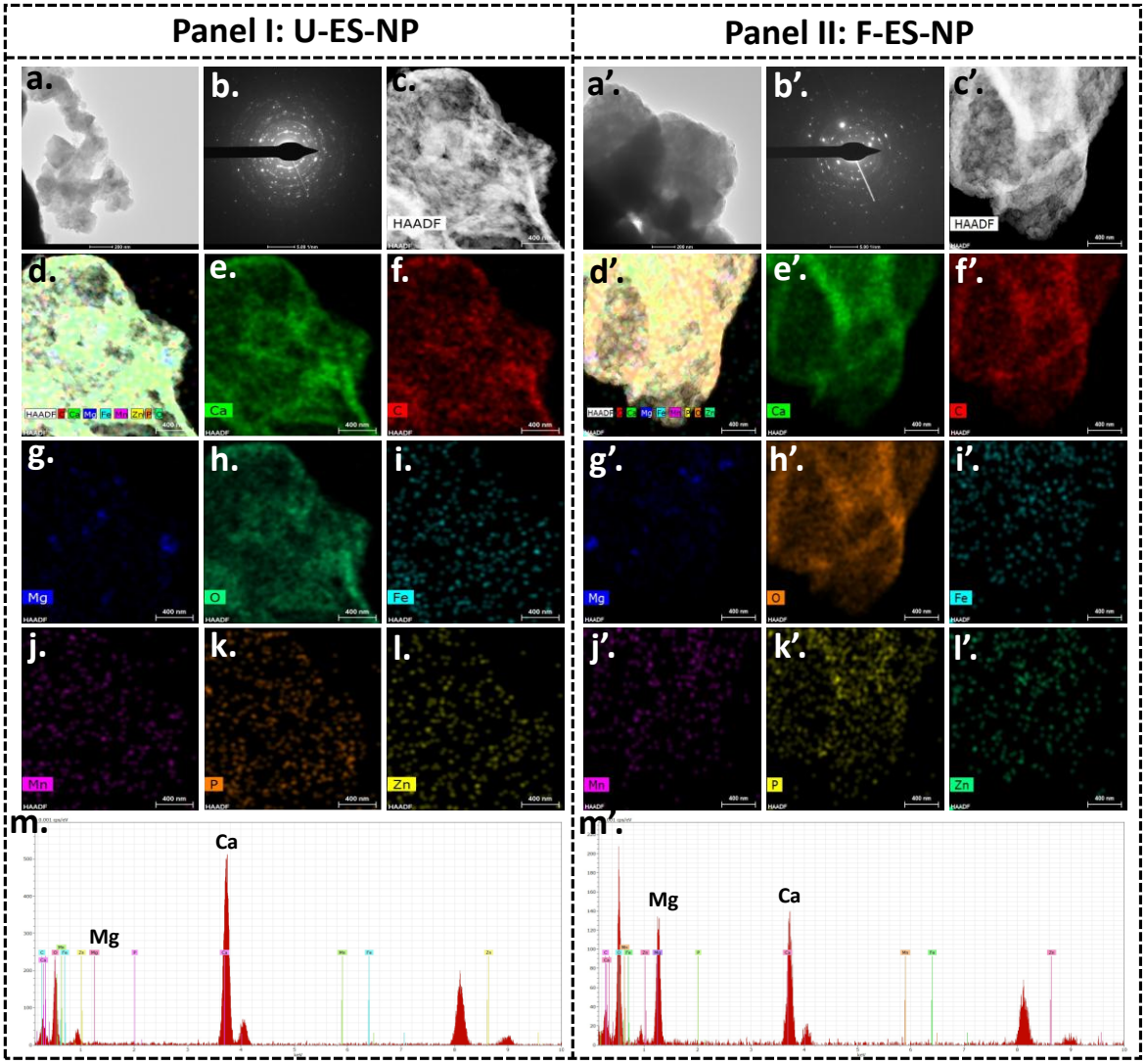

Figure S3. TEM images and EDAX analysis of: (Panel I) U-ES-NP, and (Panel II) F-ES-NP. **(a)** High magnification image of U-ES-NP (scale bar: 200 nm). **(b)** Selected area electron diffraction (SAED) pattern of U-ES-NP; **(c)** Corresponding high-angle annular dark-field (HAADF) image of U-ES-NP (scale bar: 400 nm); **(d)** Elemental mapping showing the presence of different elements in U-ES-NP indicated by different colors: **(e)** calcium (green); **(f)** carbon (red); **(g)** magnesium (deep blue); **(h)** oxygen (bluish green); **(i)** iron (sky blue); **(j)** manganese (violet); **(k)** phosphorus (orange); and **(l)** zinc (yellow). **(m)** EDAX analysis of U-ES-NP showing presence of different metals. Similarly, **(a')** High magnification image of F-ES-NP (scale bar: 200 nm). **(b')** Selected area electron diffraction (SAED) pattern of F-ES-NP; **(c')** Corresponding high-angle annular dark-field (HAADF) image of F-ES-NP (scale bar: 400 nm); **(d')** Elemental mapping showing the presence of different elements in F-ES-NP indicated by different colors: **(e')** calcium (green); **(f')** carbon (red); **(g')** magnesium (deep blue); **(h')** oxygen (orange); **(i')** iron (sky blue); **(j')** manganese (violet); **(k')** phosphorus (yellow); and **(l')** zinc (bluish green). **(m')** EDAX analysis of F-ES-NP showing presence of different metals. The results indicate that these nanoparticles are mostly composed of calcium.

Figure S4.

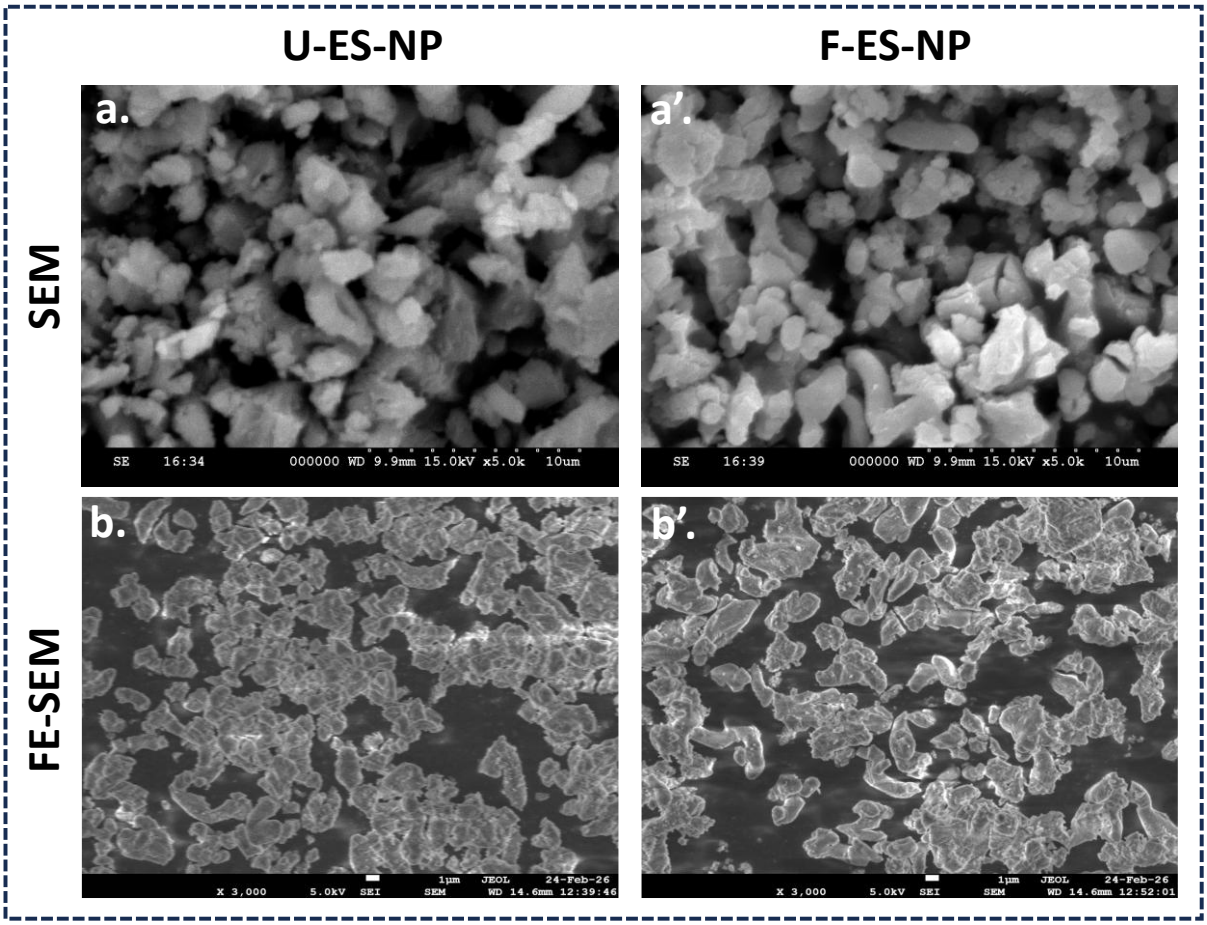

Figure S4. Representative SEM of: **(a)** U-ES-NP; and **(a')** F-ES-NP. Representative FE-SEM of: **(b)** U-ES-NP; and **(b')** F-ES-NP indicate the morphology of particles.

Figure S5.

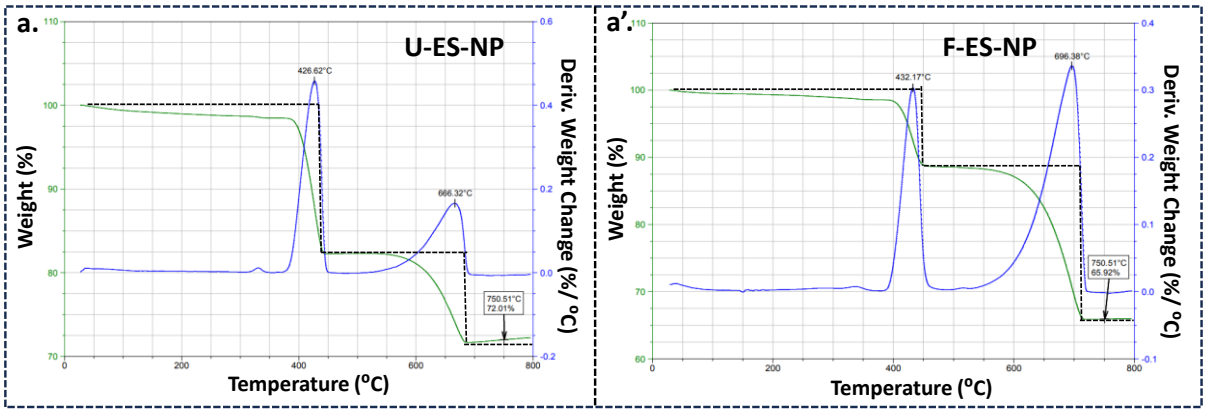

Figure S5. TGA and DTG curve analysis of: **(a)** U-ES-NP; **(a')** F-ES-NP. TGA curve of U-ES-NP and F-ES-NP shows stepwise decomposition between 25 ºC and 800 ºC indicating that these samples are thermostable in nature.

Figure S6.

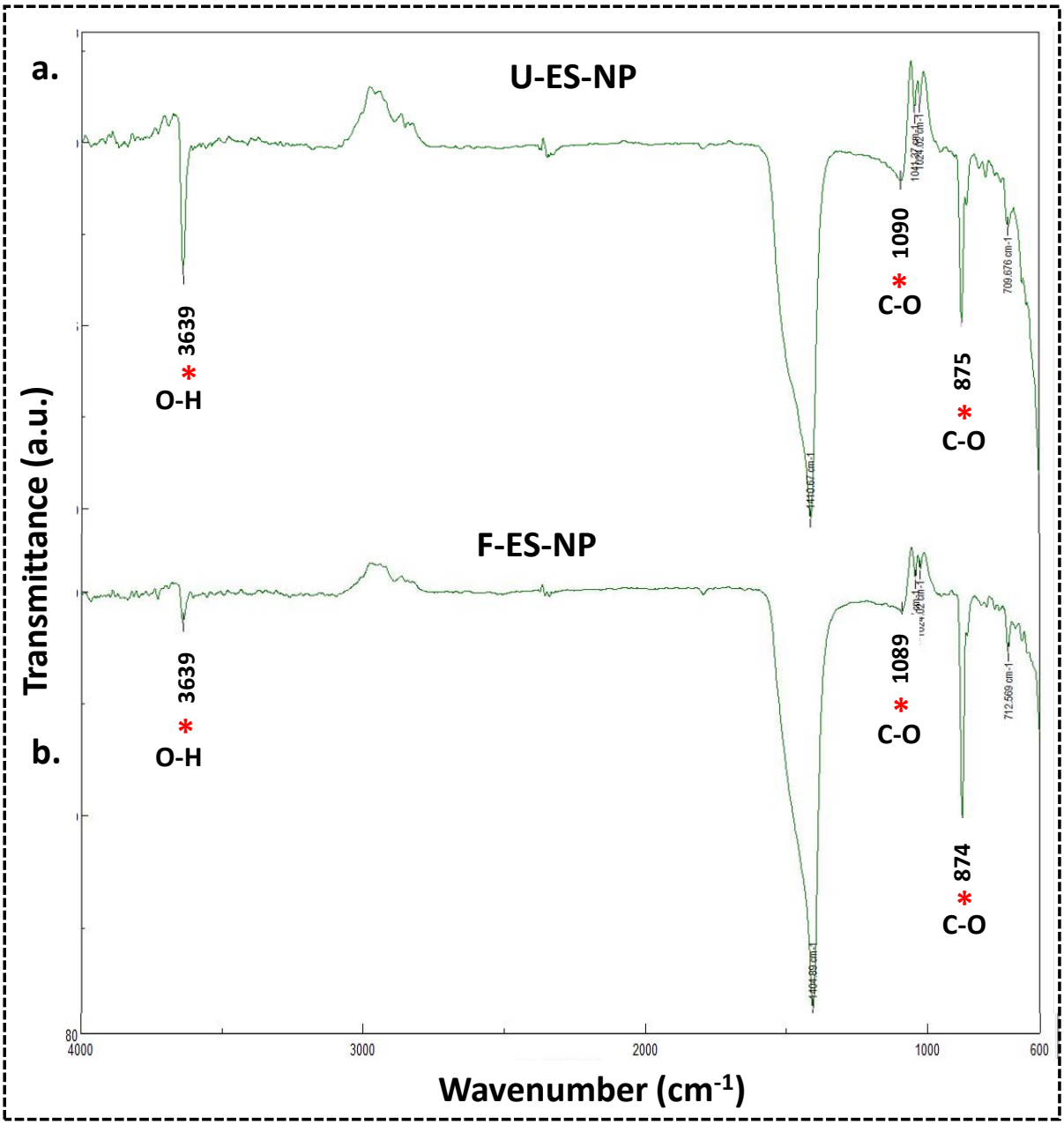

Fig S6. FT-IR spectra of: **(a)** U-ES-NP and **(b)** F-ES-NP

Figure S7

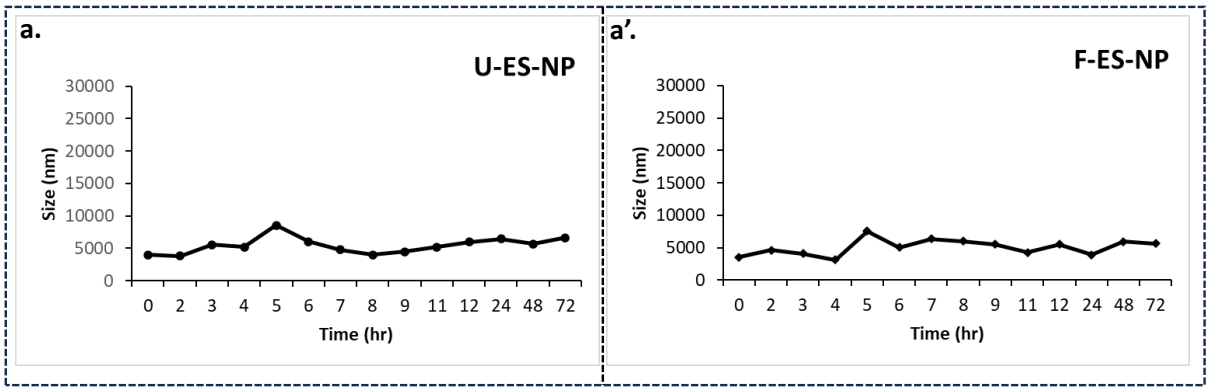

Figure S7. Time-dependent (0-72h) stability evaluation of: **(a)** U-ES-NP; **(a')** F-ES-NP, showing changes in particle size (nm) in DMEM media analyzed through DLS.

Figure S8

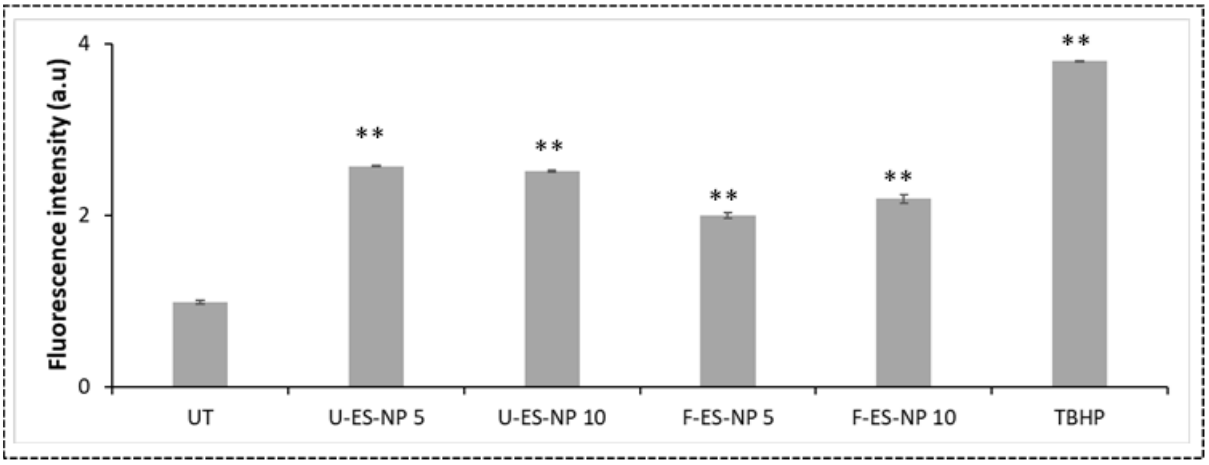

Figure S8. Quantification of the immunofluorescence of the ROS generated DCFDA in the HaCaT cells with groups UT, TBHP, U-ES-NP (5-10 µg/mL), and F-ES-NP (5-10 µg/mL). These experiments are performed thrice and represented as mean±SD. Significant differences from untreated (UT) cells are observed (**$p < 0.01$).

Figure S9.

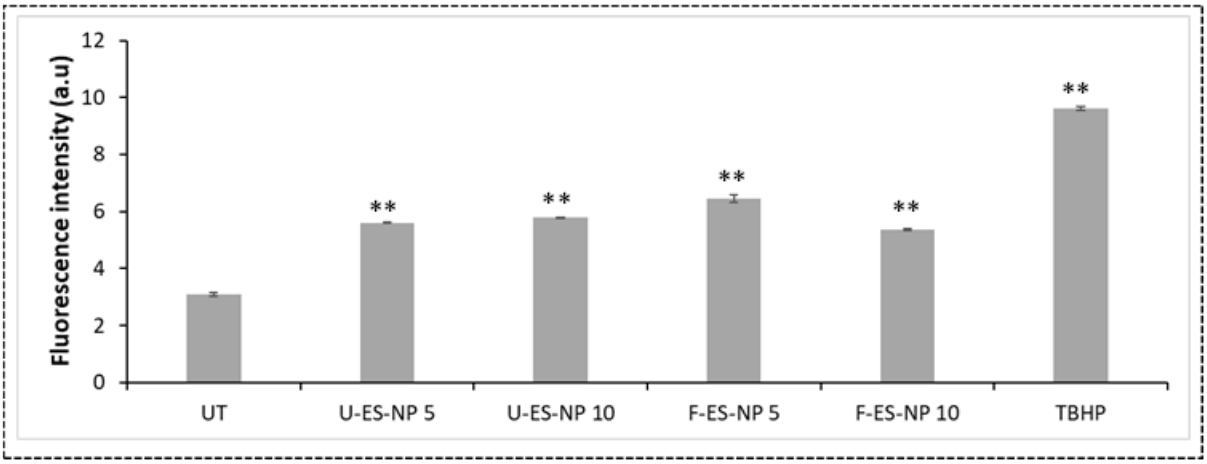

Figure S9. Quantification of the immunofluorescence of the ROS generated DHE in the HaCaT cells with groups UT, TBHP, U-ES-NP (5-10 µg/mL), and F-ES-NP (5-10 µg/mL). These experiments are performed thrice and represented as mean±SD. Significant differences from untreated (UT) cells are observed (**$p < 0.01$).

Figure S10.

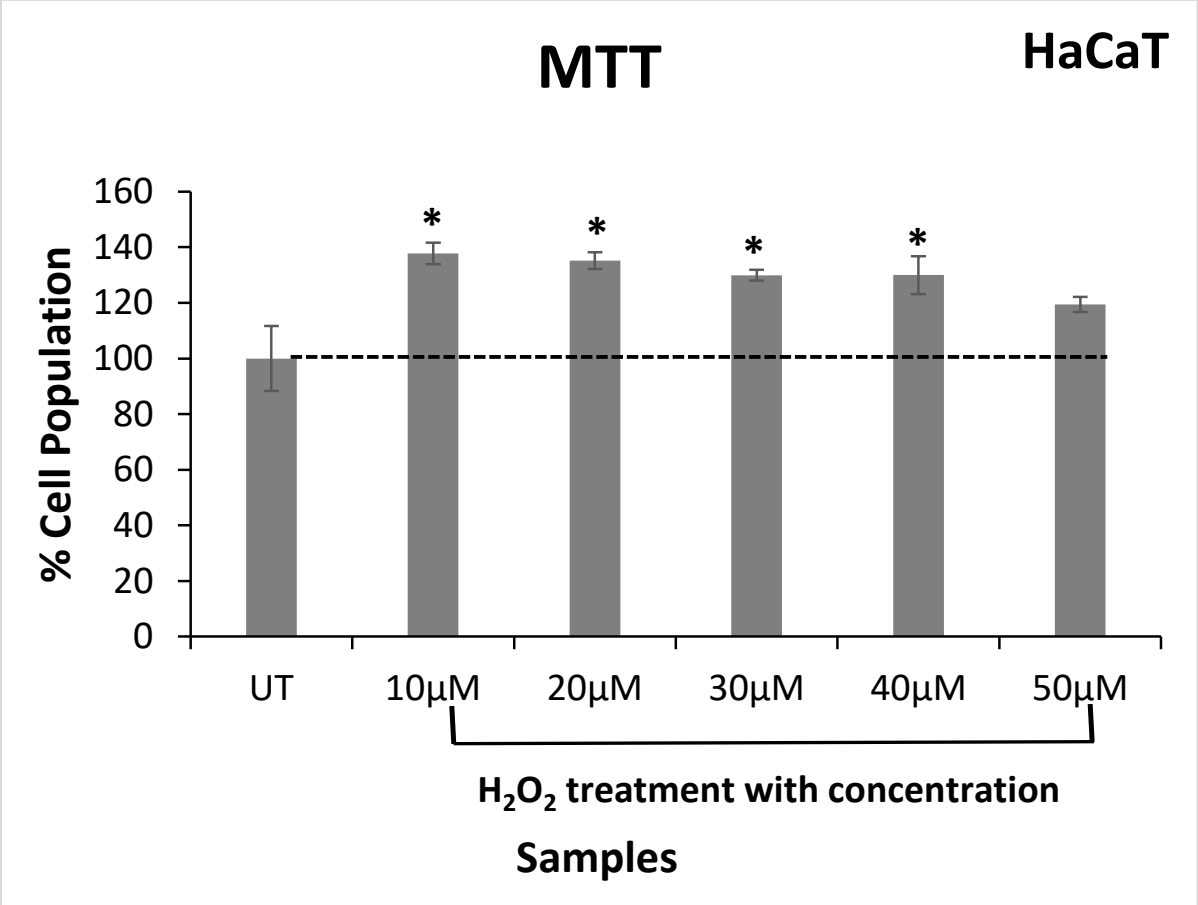

Figure S10. Cell viability assay in HaCaT cell line using H_2O_2 in a dose-dependent manner (1-20 µg/mL) for 2 h. These experiments are performed thrice and represented as mean±SD. Significant differences from untreated (UT) cells are observed (*$p < 0.05$).

Figure S11.

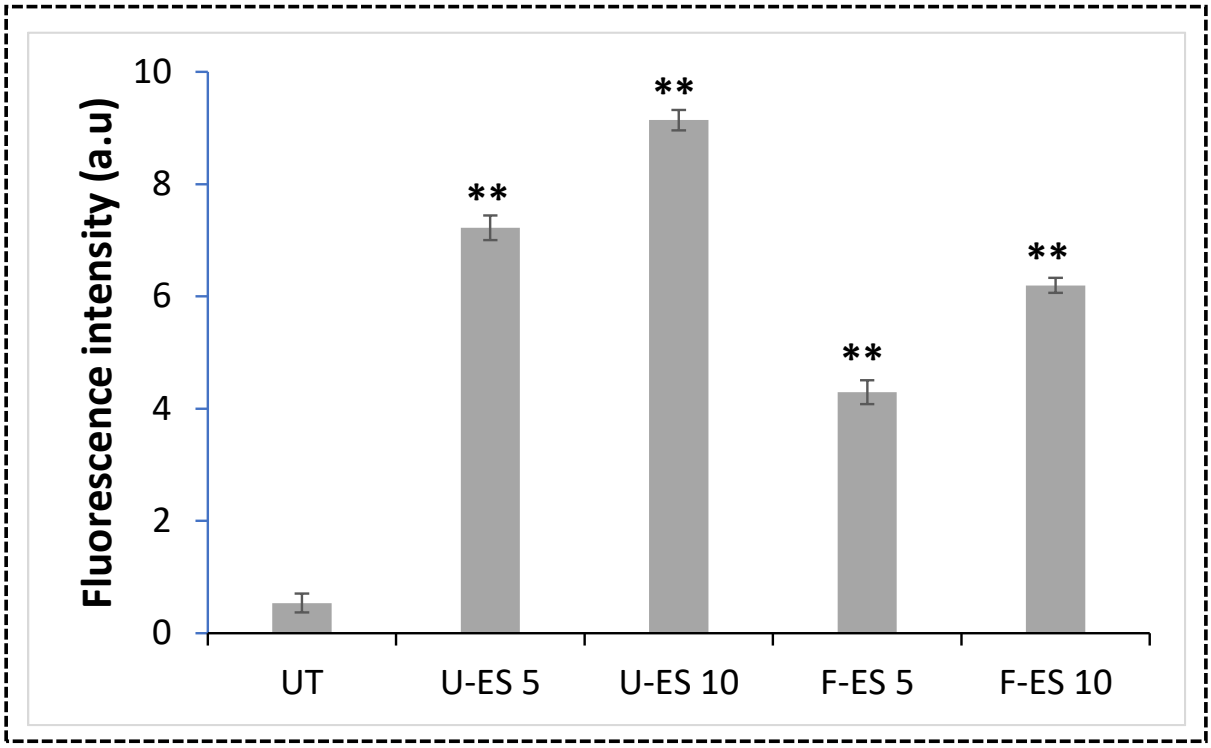

Figure S11. The quantification of the immunofluorescence images indicates higher expression of Ki-67 in the HaCaT cells treated with U-ES-NP (5-10 µg/mL) and F-ES-NP (5-10 µg/mL) as compared to the untreated (UT) control. These experiments are performed thrice and represented as mean±SD. Significant differences from untreated (UT) cells are observed (**$p < 0.01$).

Figure S12.

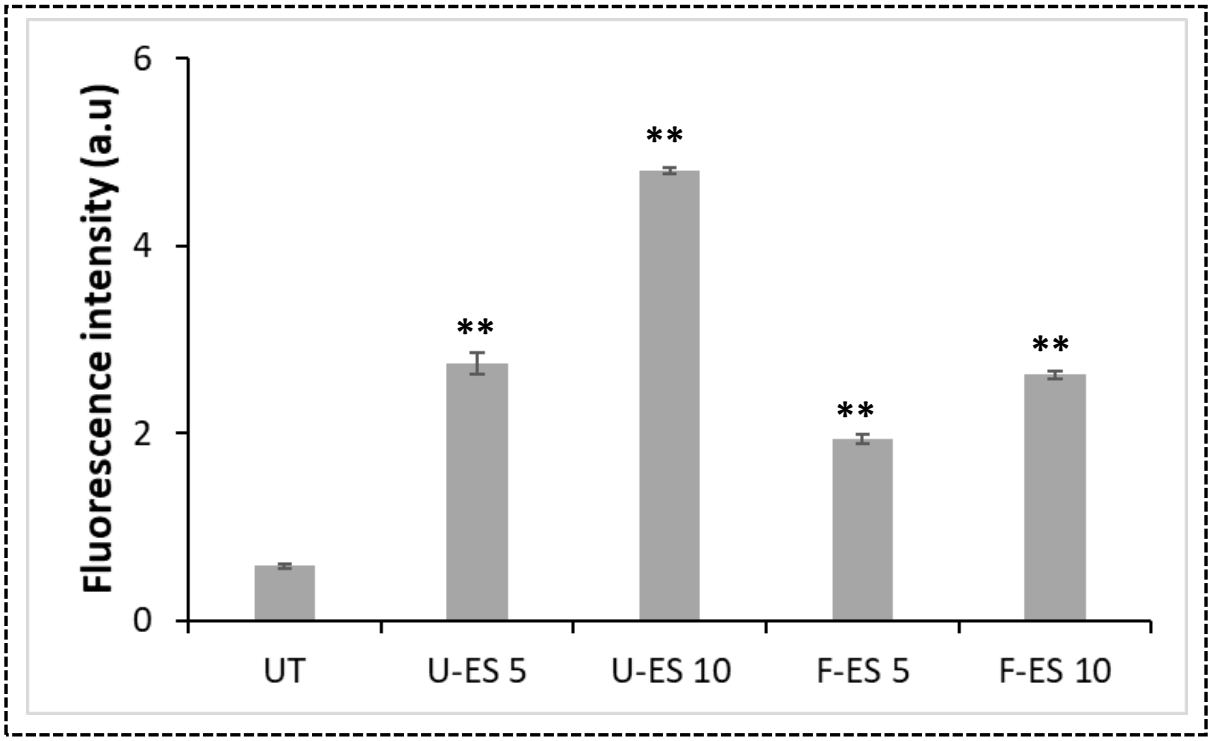

Figure S12. The quantification of the immunofluorescence images indicates higher expression of CD44 in the HaCaT cells treated with U-ES-NP (5-10 µg/mL) and F-ES-NP (5-10 µg/mL) as compared to the untreated. These experiments are performed thrice and represented as mean±SD. Significant differences from untreated (UT) cells are observed (**$p < 0.01$).

Figure S13.

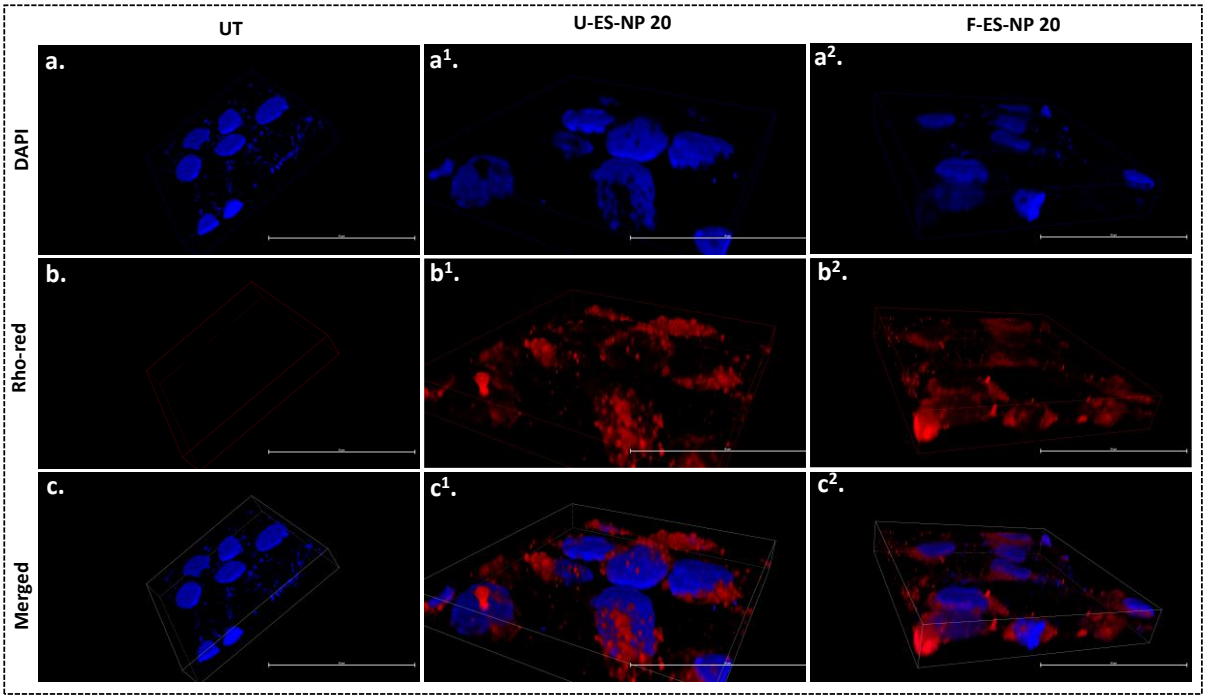

Figure S13. Representative Z-stacked images of cellular localization of rhodamine labeled ES-NP in HaCaT cells where: **(a-a^3)** DAPI (UT) control; **(b-b^3)** Rho-red; **(c-c^3)** Merged images; and **Column I**: UT; **II**: U-ES-NP: **III**: F-ES-NP. The rho-ES-NP are localized within the cells. The images were taken using confocal microscopy at 60 × magnification, scale bar: 50 µm.

Figure S14.

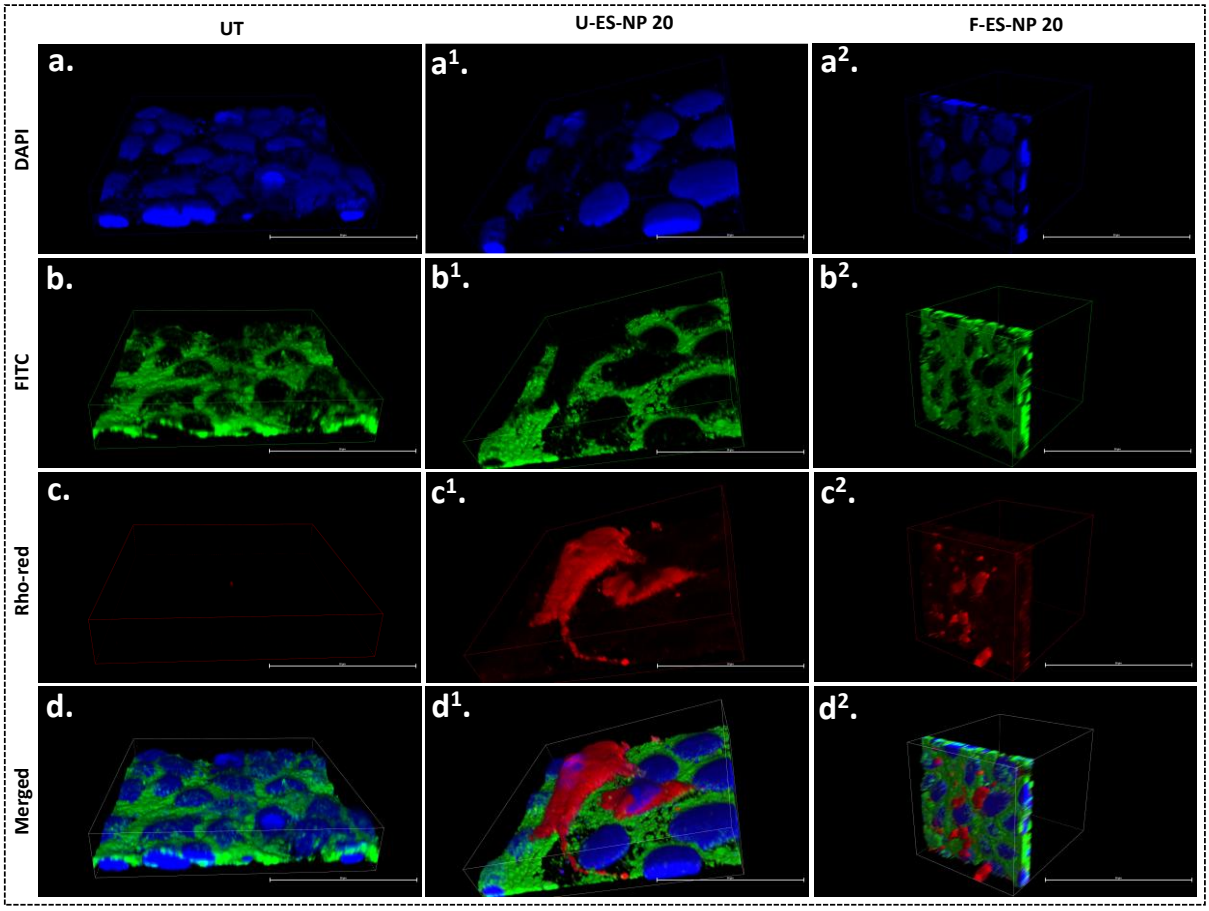

Figure S14. Representative images of cellular localization of phalloidin staining in HaCaT treated with rhodamine labeled ES-NP cells where: **(a-a^4)** DAPI (UT); **(b-b^4)** FITC; **(c-c^4)** Rho-red; **(d-d^4)** Merged images; and **Column I**: UT; **II**: U-ES-NP; **III**: F-ES-NP. The rho-incubated ES-NP in association with the actin cytoskeleton are localized within the cells. The images were taken using confocal microscopy at 60 × magnification, scale bar: 50 µm.

Scheme 1.

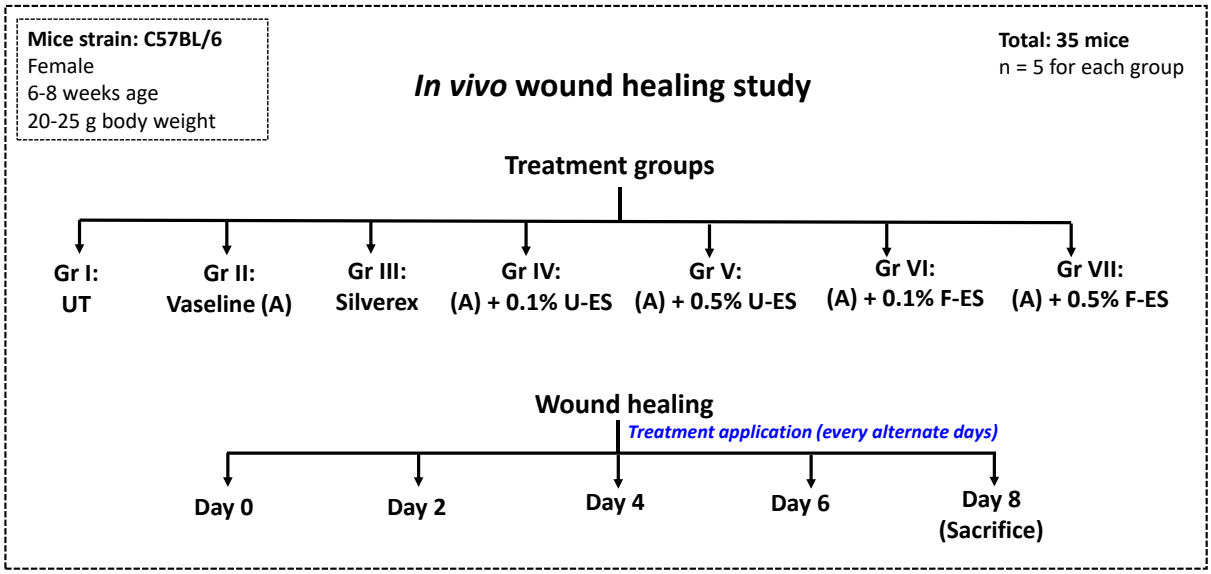

Scheme 1. Schematic representation of the experimental plan for the study of wound healing in C57BL/6 mice using ES-NP.

Figure S15a.

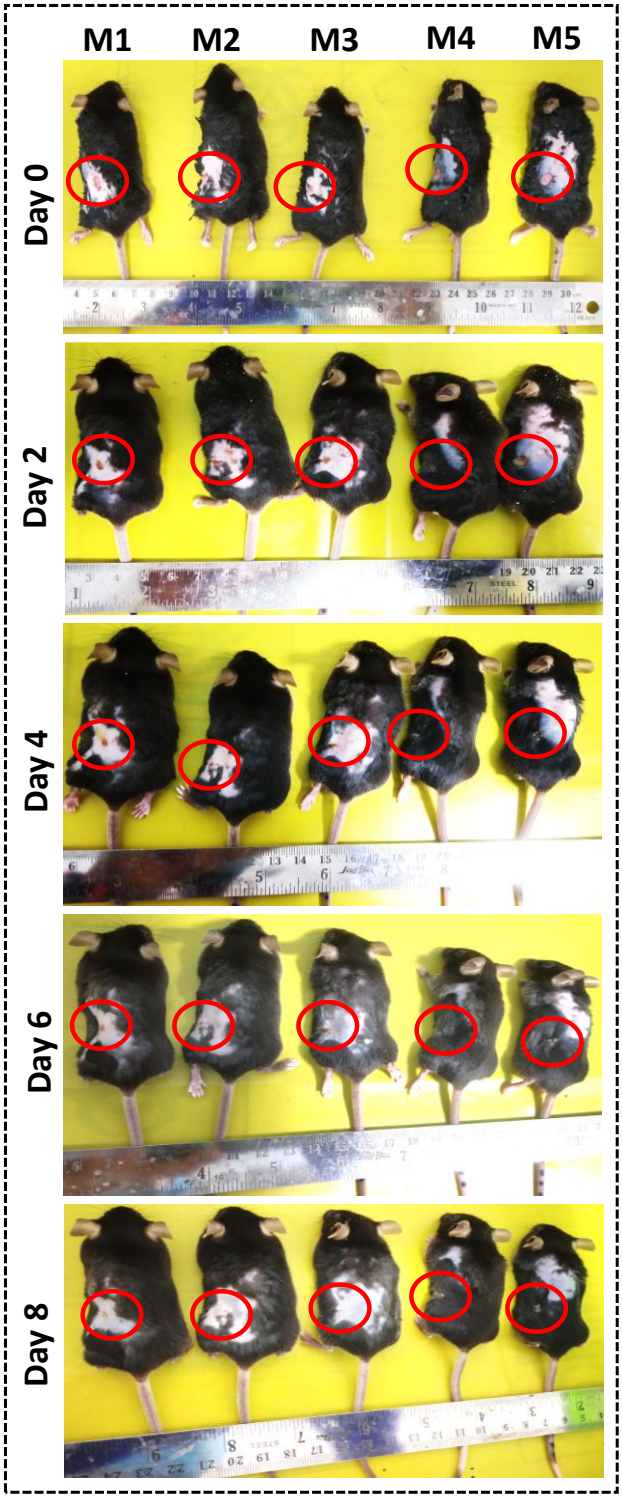

Figure S15a. Representative images of *in vivo* wound healing study of untreated (UT) group, captured at five different time points: Day 0, 2, 4, 6, and 8 in C57BL/6 mice using punch biopsy model, where the experimental groups (n = 5 for each group) are designated as Row: I: Day 0; II: Day 2; III: Day 4; IV: Day 6; and V: Day 8. Red circle encloses the wound area.

Figure S15b.

Figure S15b. Representative images of *in vivo* wound healing study of Vaseline-treated group (vehicle control), captured at five different time points: Day 0, 2, 4, 6, and 8 in C57BL/6 mice using punch biopsy model, where the experimental groups (n = 5 for each group) are designated as Row: I: Day 0; II: Day 2; III: Day 4; IV: Day 6; and V: Day 8. Red circle encloses the wound area.

Figure S15c.

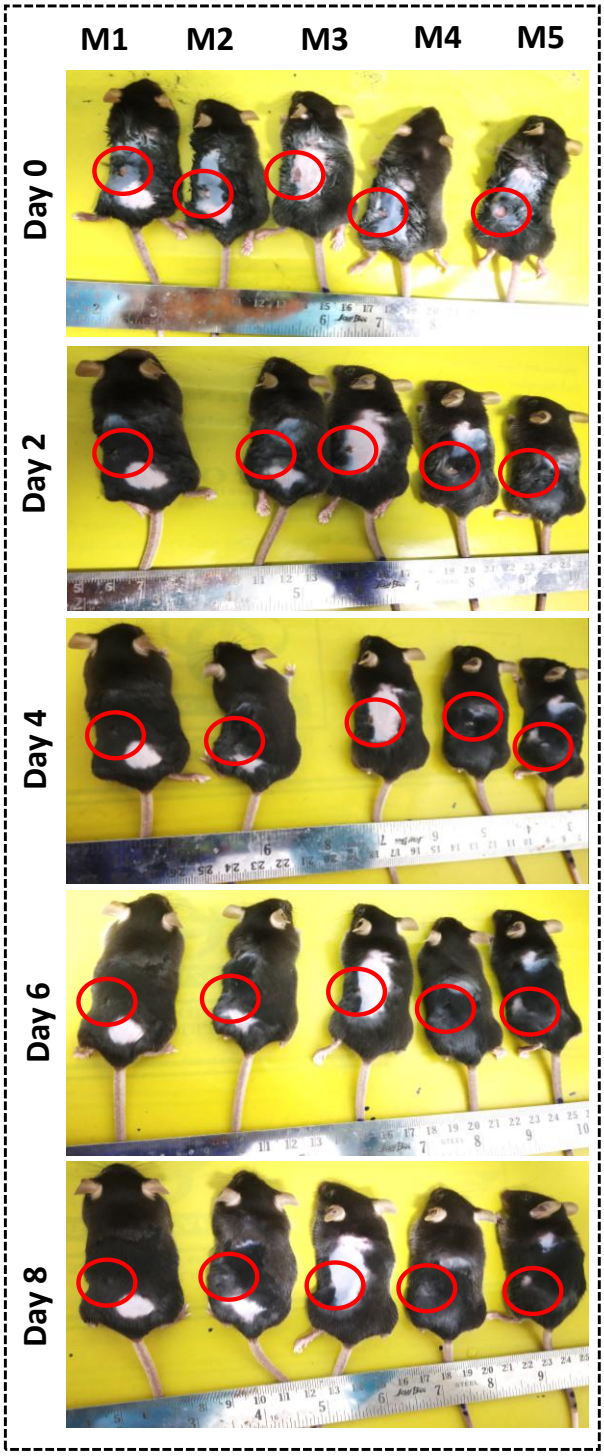

Figure S15c. Representative images of *in vivo* wound healing study of Silverex-treated group (positive control), captured at five different time points: Day 0, 2, 4, 6, and 8 in C57BL/6 mice using punch biopsy model, where the experimental groups (n = 5 for each group) are designated as Row: I: Day 0; II: Day 2; III: Day 4; IV: Day 6; and V: Day 8. Red circle encloses the wound area.

Figure S15d.

Figure S15d. Representative images of *in vivo* wound healing study of U-ES-NP (0.1%)-treated group, captured at five different time points: Day 0, 2, 4, 6, and 8 in C57BL/6 mice using punch biopsy model, where the experimental groups (n = 5 for each group) are designated as Row: I: Day 0; II: Day 2; III: Day 4; IV: Day 6; and V: Day 8. Red circle encloses the wound area.

Figure S15e.

Figure S15e. Representative images of *in vivo* wound healing study of U-ES-NP (0.5%) group, captured at five different time points: Day 0, 2, 4, 6, and 8 in C57BL/6 mice using punch biopsy model, where the experimental groups (n = 5 for each group) are designated as Row: I: Day 0; II: Day 2; III: Day 4; IV: Day 6; and V: Day 8. Red circle encloses the wound area.

Figure S15f.

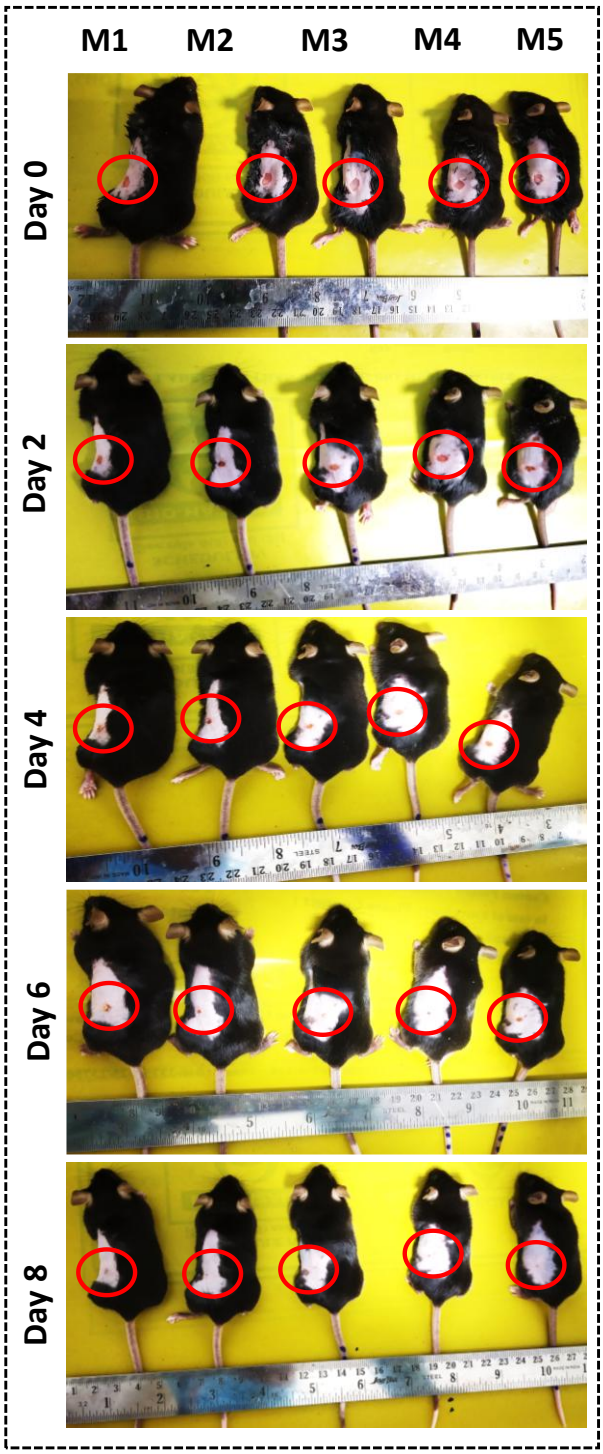

Figure S15f. Representative images of *in vivo* wound healing study of F-ES-NP (0.1%)-treated group, captured at five different time points: Day 0, 2, 4, 6, and 8 in C57BL/6 mice using punch biopsy model, where the experimental groups (n = 5 for each group) are designated as Row: I: Day 0; II: Day 2; III: Day 4; IV: Day 6; and V: Day 8. Red circle encloses the wound area.

Figure S15g.

Figure S15g. Representative images of *in vivo* wound healing study of F-ES-NP (0.5%)-treated group, captured at five different time points: Day 0, 2, 4, 6, and 8 in C57BL/6 mice using punch biopsy model, where the experimental groups (n = 5 for each group) are designated as Row: I: Day 0; II: Day 2; III: Day 4; IV: Day 6; and V: Day 8. Red circle encloses the wound area.

Figure S16.

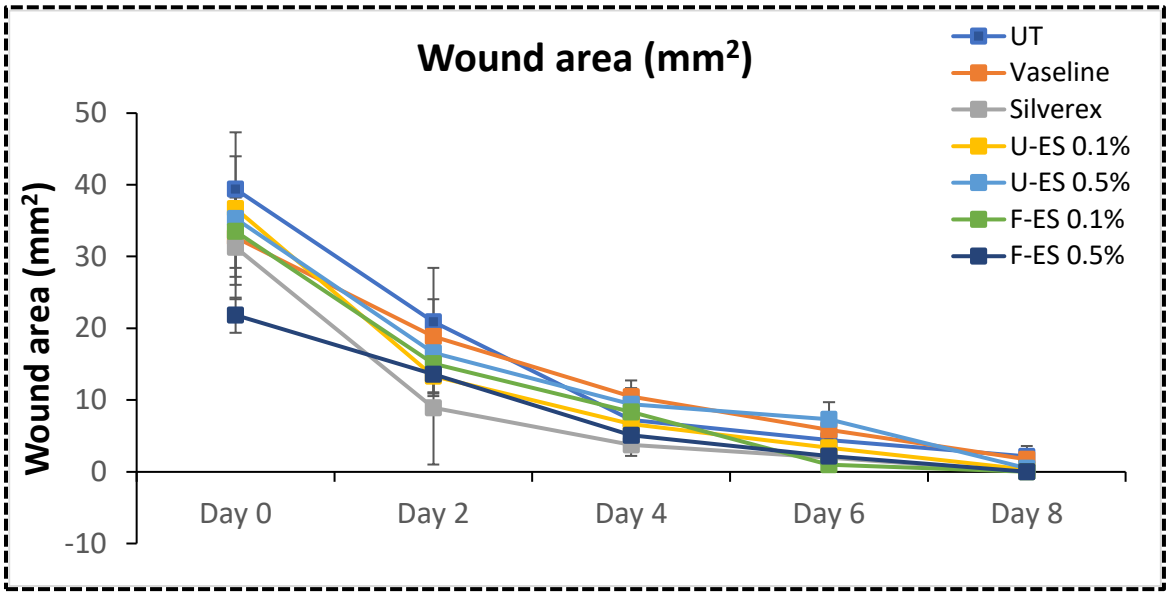

Figure S16. Corresponding quantification of wound closure in C57BL/6J mice with different treatments (UT, Vaseline, 0.1% and 0.5% U-ES-NP, 0.1% and 0.5% F-ES-NP, and Silverex) using Vernier calipers. The results clearly show the accelerated wound healing in mouse treated with U-ES-NP and F-ES-NP compared to untreated (UT) control.

Figure S17.

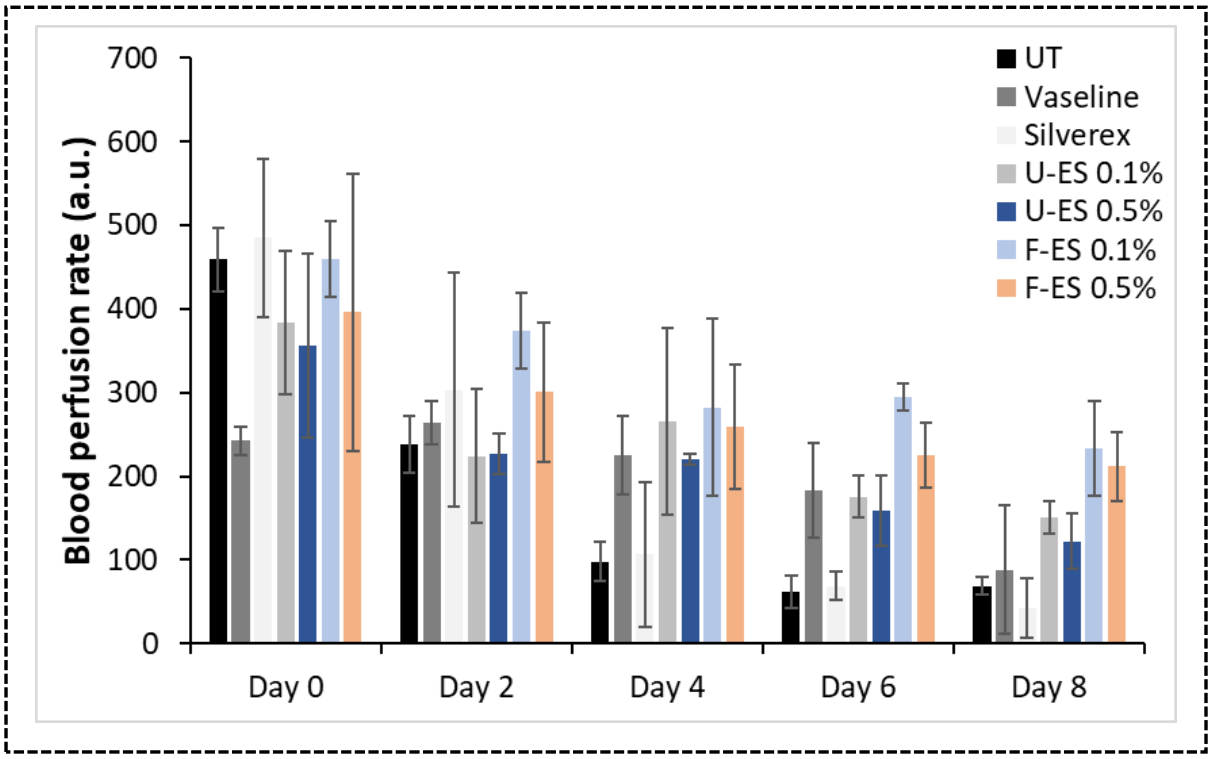

Figure S17. Blood perfusion rate of C57BL/6J mice with different treatments (UT, Vaseline, 0.1% and 0.5% U-ES-NP, 0.1% and 0.5% F-ES-NP, and Silverex) for analysing wound closure using LDI.

Figure S18.

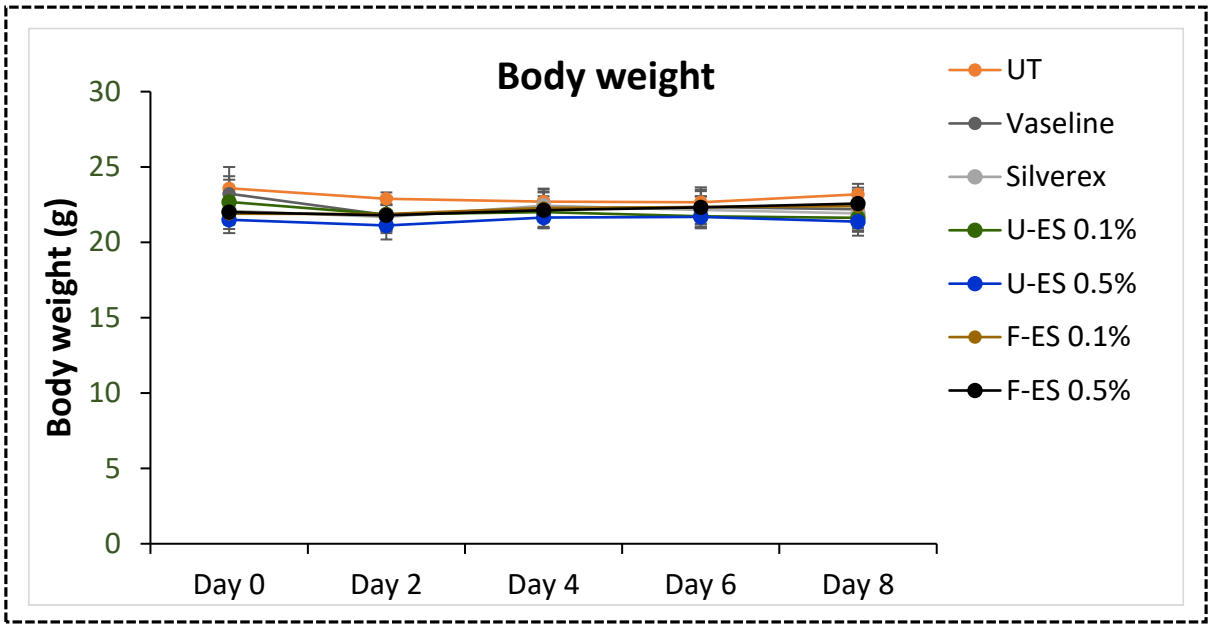

Figure S18. Time dependent variation in body weight of all the groups (UT, Vaseline, 0.1% and 0.5% U-ES-NP, and 0.1% and 0.5% F-ES-NP, and Silverex) of mice indicating no change in body weight of U-ES-NP and F-ES-NP treated group with respect to untreated (UT) control.

Figure S19.

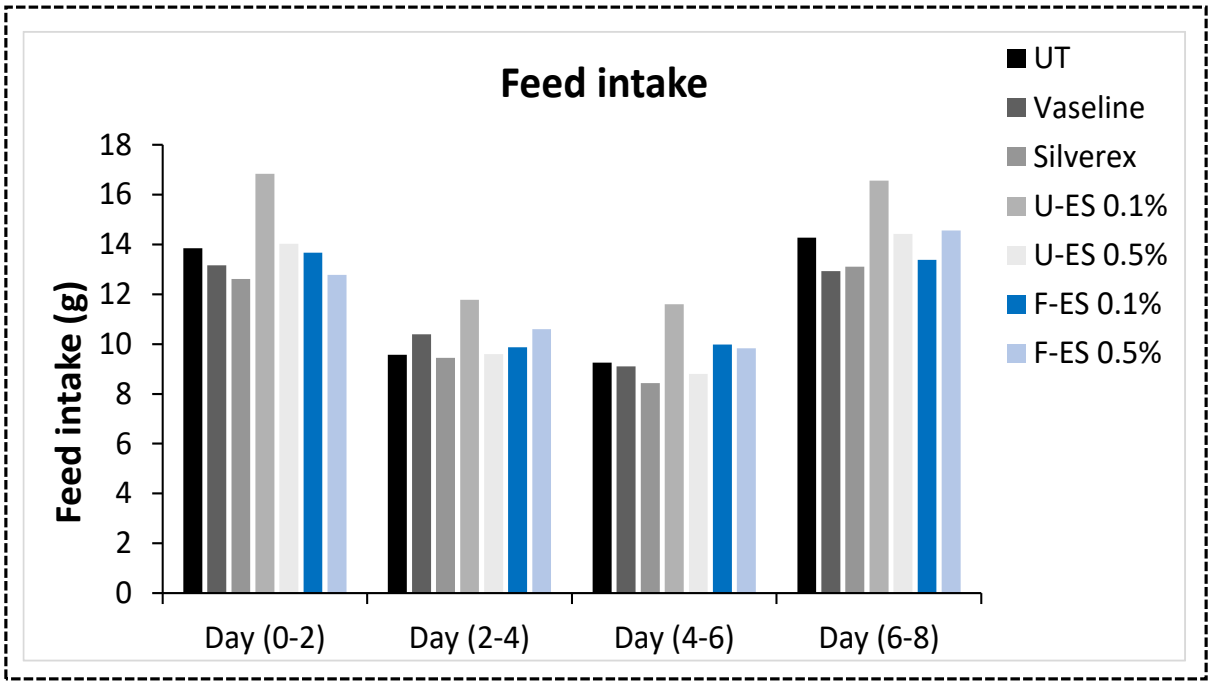

Figure S19. Time dependent variation in feed weight of all the groups (UT, Vaseline, 0.1% and 0.5% U-ES-NP, 0.1% and 0.5% F-ES-NP, and Silverex) of mice indicating same trend in feed weight of U-ES-NP and F-ES-NP treated group with respect to untreated (UT) control.

Figure S20.

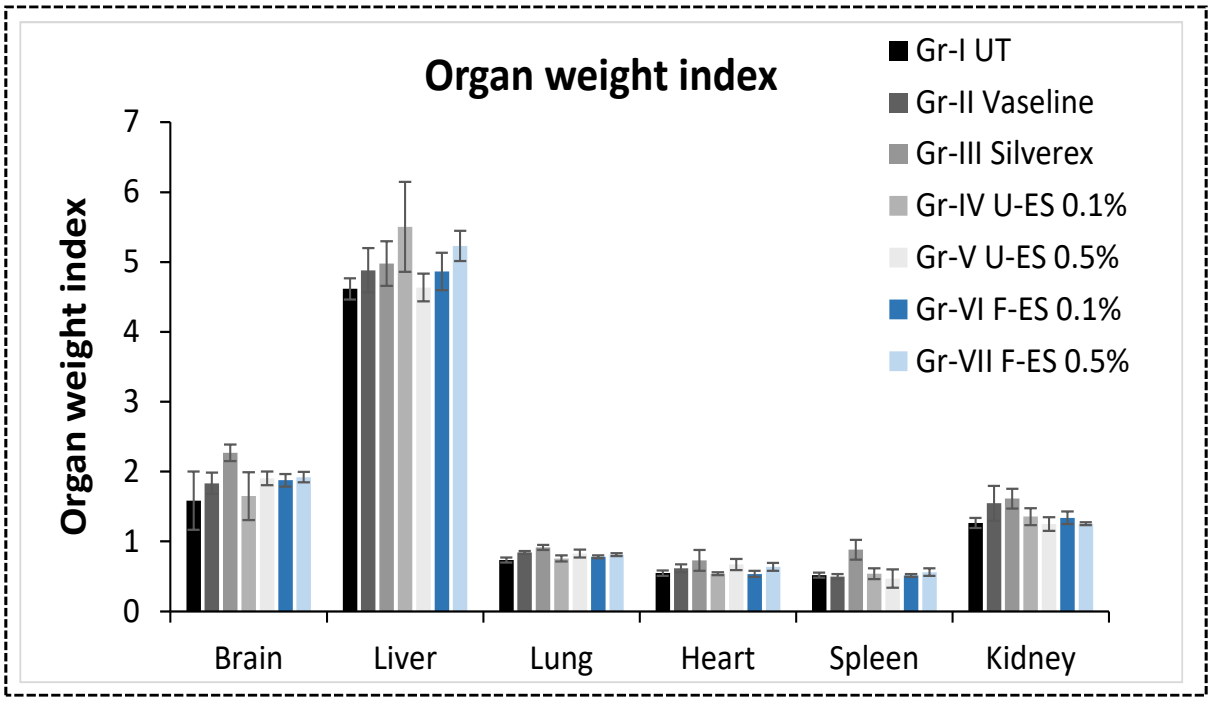

Figure S20. Variation in organ weight index of all the groups (UT, Vaseline, 0.1% and 0.5% U-ES-NP, 0.1% and 0.5% F-ES-NP, and Silverex) after sacrifice of the mice indicating no change in organ weight index of U-ES-NP and F-ES-NP treated group with respect to untreated (UT).

Figure S21.

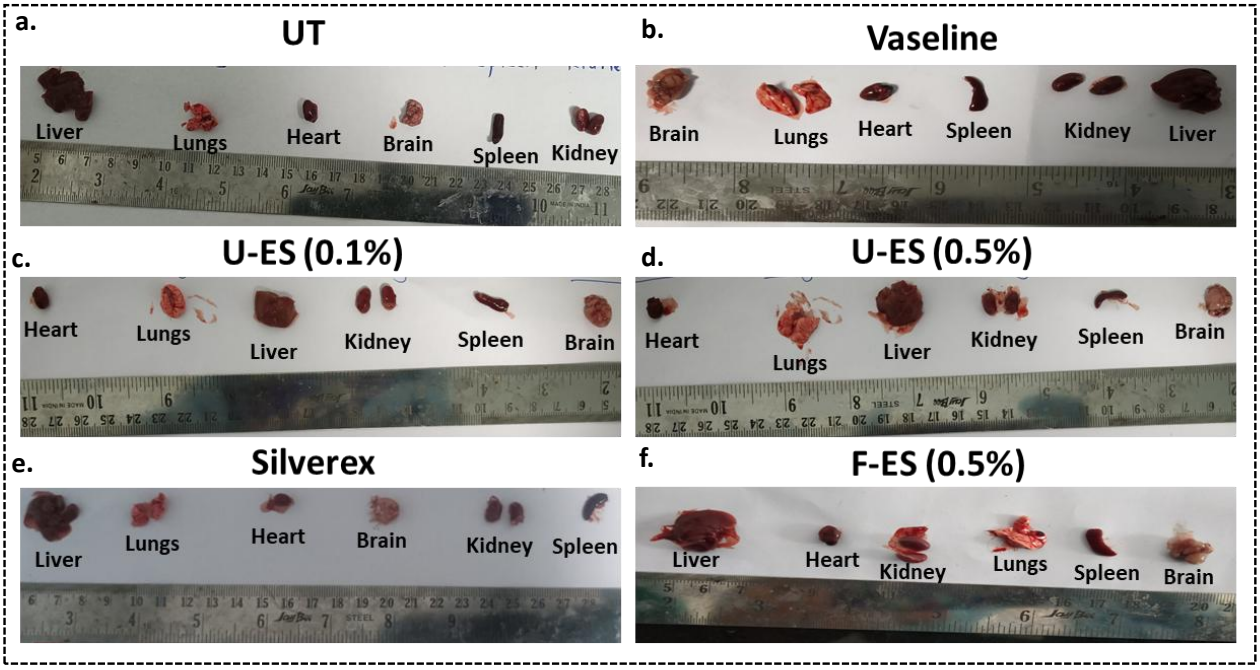

Figure S21. Representative images of the major organs (liver, lungs, heart, brain, spleen, and kidney) in mice after sacrifice for all the groups (UT, Vaseline, 0.1% & 0.5% U-ES-NP, 0.5% F-ES-NP, and Silverex) indicating no significant observable changes in the major organs of U-ES-NP and F-ES-NP treated group with respect to untreated (UT) control.

Figure S22.

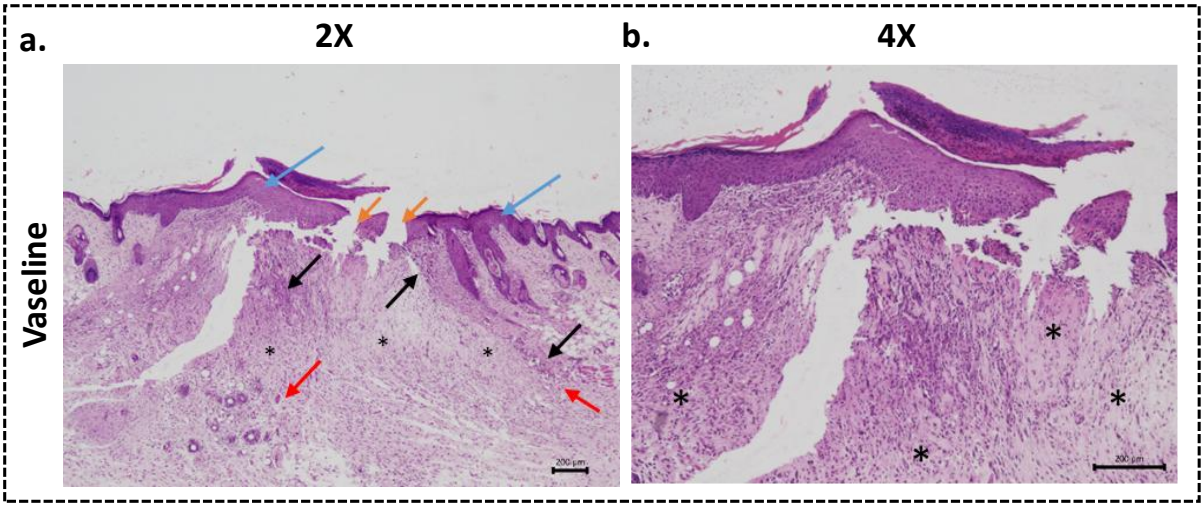

Figure S22. Histopathological analysis of isolated skin sections in Vaseline (vehicle control) treated group around the wound area stained with hematoxylin and eosin (H&E) at **(a)** 2×, and **(b)** 4×, (Scale bar: 200 µM). The yellow, blue, black and red arrow indicates the epithelial continuity, epidermal thickness, inflammatory cells infiltration within the dermis and angiogenesis within the dermis respectively. The asterisk indicates the fibroblast proliferation and collagen deposition.

Figure S23.

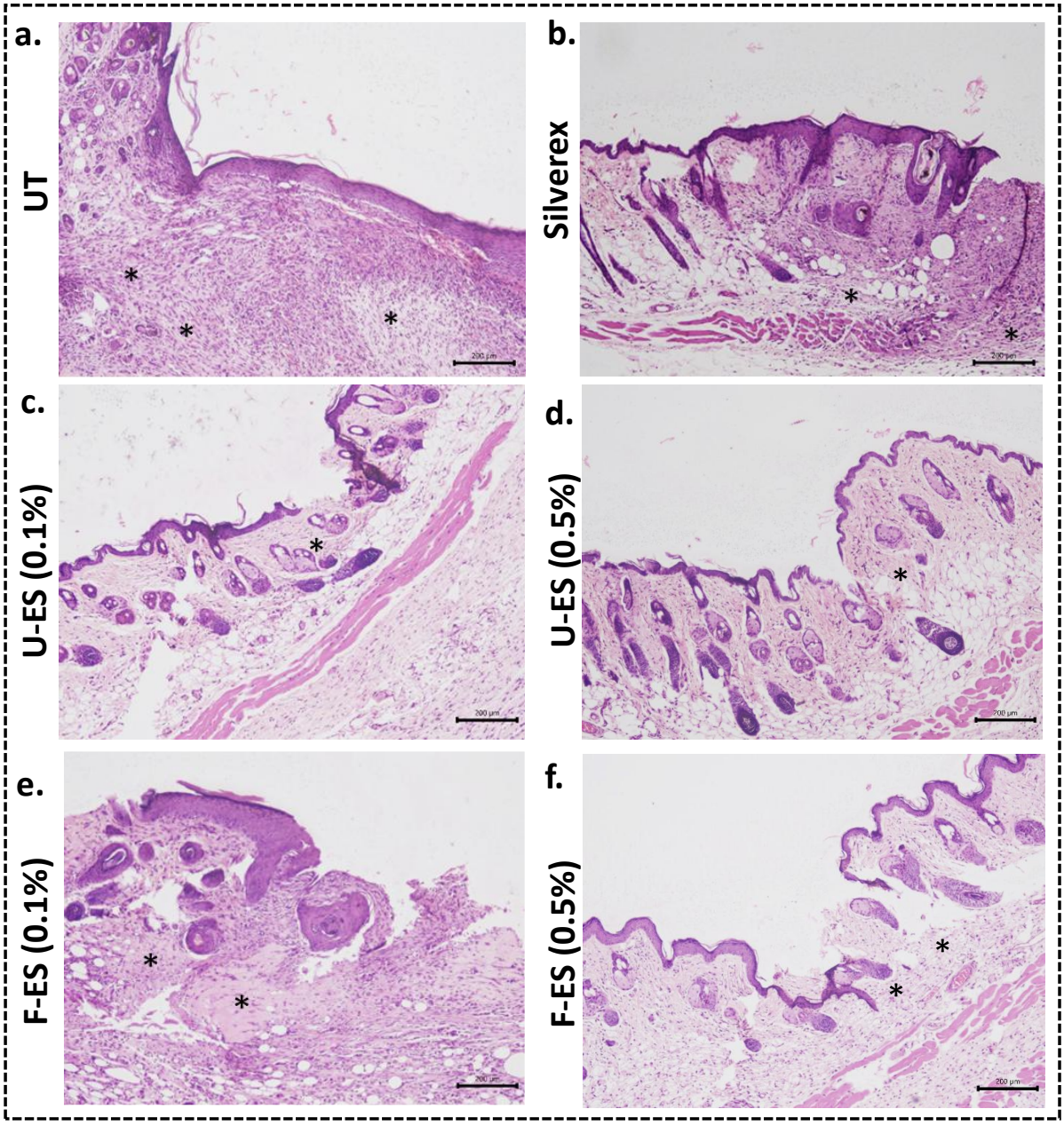

Figure S23. Histopathological analysis of isolated skin sections in around the wound area stained with hematoxylin and eosin (H&E) at 4×, (Scale bar: 200 µM), where **(a)** Untreated (UT); **(b)** Silverex (positive control); **(c)** 0.1% U-ES-NP; **(d)** 0.5% U-ES-NP; **(e)** 0.1% U-ES-NP; and **(f)** 0.5% F-ES-NP The yellow, blue, black and red arrow indicates the epithelial continuity, epidermal thickness, inflammatory cells infiltration within the dermis and angiogenesis within the dermis respectively. The asterisk indicates the fibroblast proliferation and collagen deposition.

Figure S24.

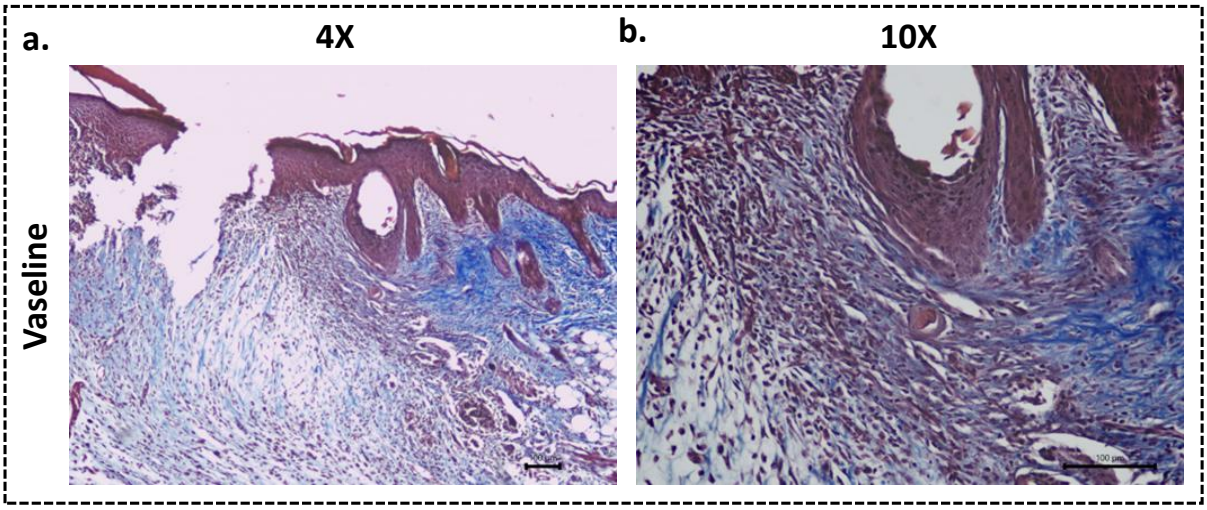

Figure S24. Histopathological analysis of isolated skin sections in around the wound area of Vaseline (vehicle control) treated group with Masson's trichrome staining, at **(a)** 4×, and **(b)** 10×; (Scale bar: 100 µM). The blue color staining indicates collagen.

Figure S25.

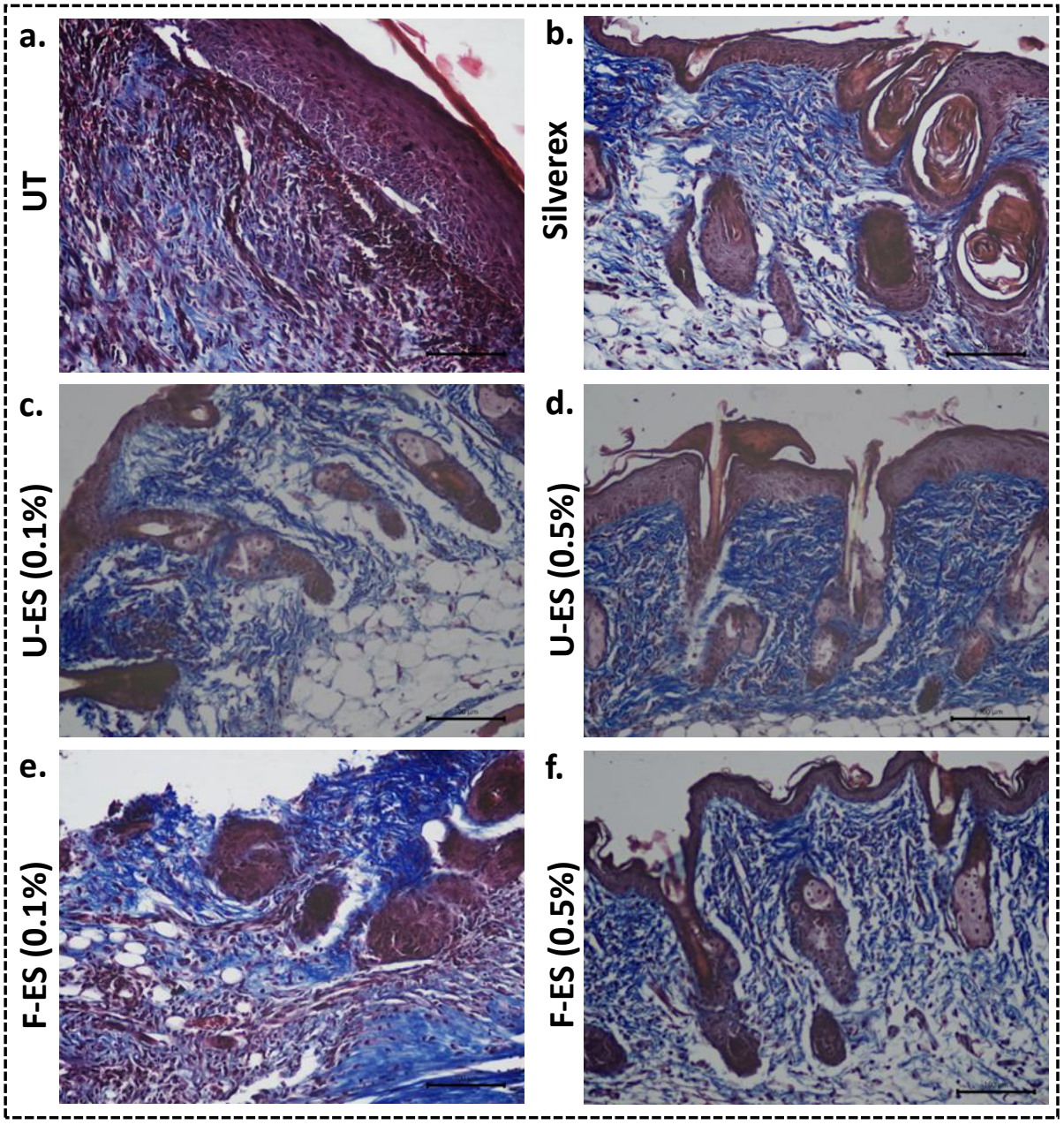

Figure S25. Histopathological analysis of isolated skin sections in around the wound area with Masson's trichrome staining, at 10×; (Scale bar: 100 µM), where **(a)** Untreated (UT); **(b)** Silverex; **(c)** 0.1% U-ES-NP; **(d)** 0.5% U-ES-NP; **(e)** 0.1% F-ES-NP; and **(f)** 0.5% F-ES-NP. The blue color staining indicates collagen.

Figure S26.

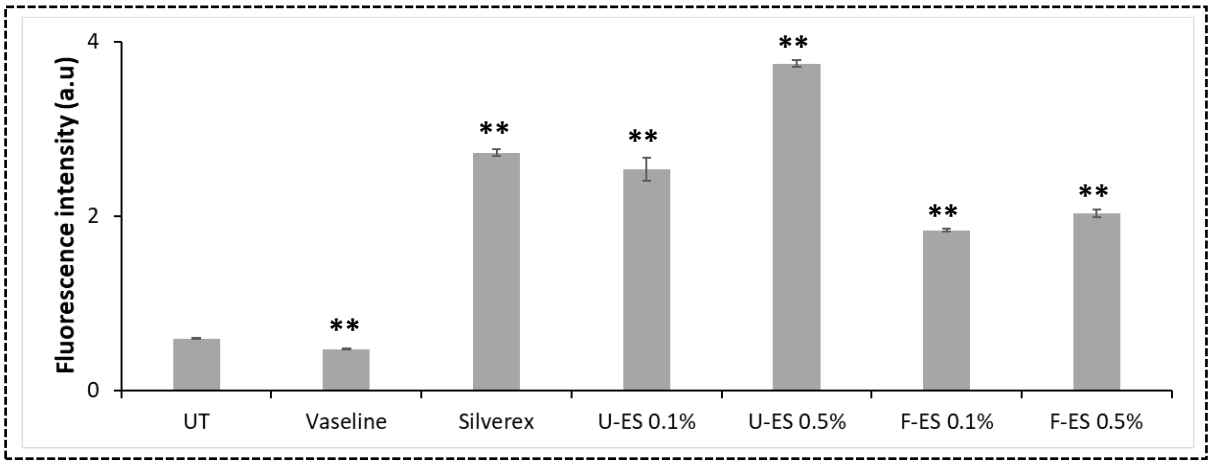

Figure S26. The quantification of the immunofluorescence images indicates higher expression of Ki-67 in the skin tissues treated with (0.1% and 0.5%) U-ES-NP, and (0.1% and 0.5%) F-ES-NP as compared to the untreated (UT) tissues; significant differences from untreated (UT) control are observed (**$p < 0.01$).

Figure S27.

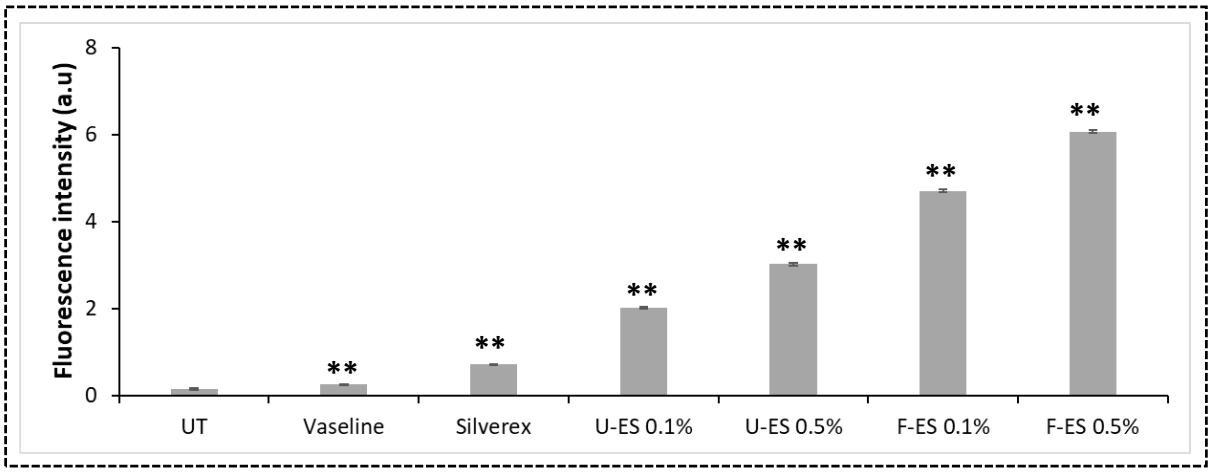

Figure S27. The quantification of the immunofluorescence images indicates higher expression of PECAM-1/CD31 in the skin tissues treated with (0.1% and 0.5%) U-ES-NP, and (0.1% and 0.5%) F-ES-NP as compared to the untreated (UT) tissues; significant differences from untreated (UT) cells are observed (**$p < 0.01$).

3. References

1. P. Nagchowdhury, S. Haque, U. Patra, S. Londhe, R. Banerjee and C. R. Patra, *Biomed. Mater.*, 2025, **20**, 045013.
2. S. Haque, R. Kotcherlakota, P. Bhamidipati, K. Muralidharan, B. Sreedhar, R. Amanchy and C. R. Patra, *Adv. Ther.*, 2023, **6**, 2300142.